

# Fabrication of Plasmonic Indium Tin Oxide Nanoparticles by Means of a Gas Aggregation Cluster Source

Artem Shelemin, Zdenek Krtous, Bill Baloukas, Oleg Zabeida, Jolanta Klemberg-Sapieha, and Ludvik Martinu\*



Cite This: *ACS Omega* 2023, 8, 6052–6058



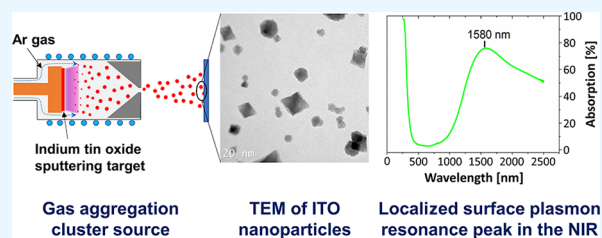
Read Online

ACCESS |

Metrics & More

Article Recommendations

**ABSTRACT:** In this work, we demonstrate, for the first time, the possibility to fabricate indium tin oxide nanoparticles (ITO NPs) using a gas aggregation cluster source. A stable and reproducible deposition rate of ITO NPs has been achieved using magnetron sputtering of an  $\text{In}_2\text{O}_3/\text{SnO}_2$  target (90/10 wt %) at an elevated pressure of argon. Remarkably, most of the generated NPs possess a crystalline structure identical to the original target material, which, in combination with their average size of 17 nm, resulted in a localized surface plasmon resonance peak at 1580 nm in the near-infrared region.



## INTRODUCTION

The outstanding combination of high luminous transmission (70–90%) in the visible part of the spectrum and low resistivity (down to  $10^{-4} \Omega\cdot\text{cm}$ ) has made indium tin oxide (ITO) an indispensable part of many optoelectronic applications such as light-emitting diodes,<sup>1</sup> liquid crystal and touch screen displays,<sup>2</sup> and electrochromic<sup>3</sup> and photovoltaic systems.<sup>4,5</sup> Such prominent properties are particularly inherent to ITO thin films, the thickness of which varies from a few nanometers up to several microns. For this goal, several fabrication methods have been developed based on wet-chemistry syntheses<sup>6–8</sup> (sol–gel, spin-coating, etc.) and physical vapor deposition<sup>9–11</sup> (e-beam evaporation, pulsed laser deposition, magnetron sputtering, etc.).

Recent advances in nanotechnology have demonstrated excellent prospects for another form of ITO material, namely, nanoparticles (NPs). One of the most exciting properties of such ITO NPs is their ability to generate a localized surface plasmon resonance (LSPR) peak in the near-infrared region<sup>12</sup> without affecting the luminous transmission in the visible region. Similar to other plasmonic materials such as noble metal NPs, the frequency of the LSPR can be tuned by adjusting the size and shape of the ITO NPs and the properties of the surrounding medium.<sup>13</sup> In addition, ITO NPs possess the exclusive property of tuning the LSPR peak position by changing their chemical composition, mainly by controlling the concentration of Sn<sup>14–16</sup> or oxygen vacancies.<sup>17</sup> Therefore, ITO NPs are particularly interesting for applications suitable for robust infrared shielding without mitigating visible light transmittance<sup>18</sup> such as electrochromic smart windows<sup>19,20</sup> or automotive glass.<sup>14</sup>

Despite the many advantages of ITO NPs, there are still significant challenges regarding the integration of the currently available deposition methods with industrial manufacturing processes. For instance, the large-scale industrial production of optical coatings most often relies on vacuum-based deposition methods and is not compatible with the widely developed wet-chemistry approaches<sup>6,8,13,14,18,19,21</sup> for synthesizing ITO NPs. Moreover, to the best of our knowledge, there are no alternative vacuum-compatible deposition processes for ITO NPs<sup>22</sup> despite the wide use of physical vapor deposition (PVD) techniques for ITO films.

In this work, we present a simple, low-cost way of synthesizing ITO NPs using a gas aggregation cluster source (GAS). In contrast to other methods, this technique is based on magnetron sputtering and can easily be installed on any vacuum deposition chamber. It has been successfully tested in the past for the fabrication of heterogeneous metal,<sup>23–25</sup> metal-oxide,<sup>26</sup> and organic<sup>27–30</sup> NPs as well as more advanced metal–metal<sup>31,32</sup> or metal–organic<sup>33,34</sup> core–shell NPs. Another of the advantages of the GAS deposition technique is that the particles can be deposited on any substrate material compatible with high vacuum.

In this short paper, we demonstrate the applicability of the GAS method for the deposition of ITO NPs. We particularly focus on the description of the general principles of the GAS

**Received:** December 19, 2022

**Accepted:** January 12, 2023

**Published:** February 1, 2023



method with a subsequent discussion of the basic characteristics of the resulting ITO NPs.

## EXPERIMENTAL METHODOLOGY

**NP Fabrication System.** The ITO NPs were fabricated using a GAS, as illustrated in Figure 1. The cluster source

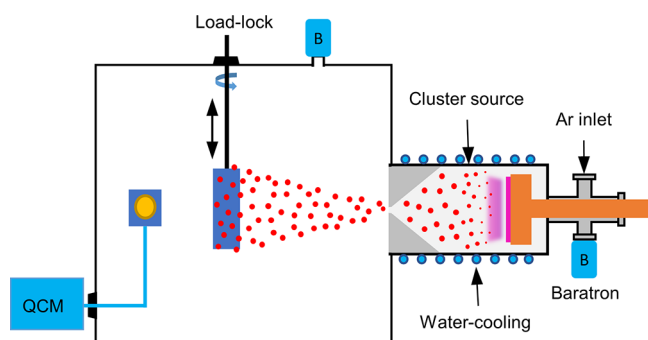


**Figure 1.** Illustration of the deposition system consisting of the GAS module mounted onto the main deposition chamber.

consists of a water-cooled cylindrical stainless-steel chamber equipped with a conical-shaped lid with a replaceable orifice. A 2 inch diameter  $\text{In}_2\text{O}_3/\text{SnO}_2$  (90/10 wt %, 99.99% pure, Kurt J. Lesker Co., PA, USA) target mounted onto a magnetron was used as the source of the material for NPs. In addition, the cluster source chamber is equipped with two ports used for a pressure gauge and a gas inlet.

The whole GAS setup was mounted on the main deposition chamber with a base pressure of around  $1 \times 10^{-4}$  Pa. The cluster source is evacuated through a few millimeters in diameter orifice utilizing the pumping system of the main chamber consisting of rotary and turbomolecular pumps. Sputtering of the ITO target was performed in the DC regime using a Pinnacle (Advanced Energy, CO, USA) power supply at different target currents from 100 to 500 mA. Argon gas (99.999% pure, Air Liquide, QC, Canada) with a flow from 7 to 25 sccm (standard cubic centimeters per minute) was introduced from behind the magnetron to improve the uniformity of the gas distribution. Ar was used as a working gas for the magnetron sputtering process but also as a

condensation center for the metal atoms.<sup>35</sup> Due to the small orifice's diameter, the Ar flowing through the cluster source creates a significant pressure differential, which, in this work, varied between 66 and 172 Pa in the GAS chamber versus 10 Pa in the main deposition chamber, which was kept constant during all experiments. The shape and the diameter of the orifice also control the speed at which NPs leave the GAS source as well as their angular spread. More details on the capabilities of the GAS method can be found elsewhere.<sup>23,29,35</sup>

The depositions of ITO NPs were performed on a nonheated substrate placed in the center of the chamber. The experimental conditions were optimized using the real-time data on the mass flux monitored by a quartz crystal microbalance (QCM), positioned about 25 cm from the orifice in the deposition chamber. The QCM's output in Hz/min was converted to more representative mass flux data using the Sauerbrey method.<sup>36</sup>

**Characterization of the NPs.** The transmission ( $T$ ), reflection ( $R$ ), and scattering ( $S$ ) spectra were measured using a Lambda 1050 (PerkinElmer Inc., MA, USA) spectrophotometer equipped with an integrating sphere (150 mm in diameter), while the absorption ( $A$ ) was calculated as  $100 - T_{\text{total}} - R_{\text{total}}$ , where  $T_{\text{total}}$  and  $R_{\text{total}}$  correspond to  $T_{\text{specular}} + T_{\text{diffuse}}$  and  $R_{\text{specular}} + R_{\text{diffuse}}$ , respectively. The total amount of scattering ( $S$ ) was calculated as  $S = T_{\text{diffuse}} + R_{\text{diffuse}}$ , where  $T_{\text{diffuse}}$  is the diffuse transmission and  $R_{\text{diffuse}}$  is the diffuse reflection.

The morphology of the ITO NPs was studied by TEM analysis using a JEM 2100F instrument from JEOL USA Inc. (MA, USA). The field emission gun TEM (FEG TEM) was operated at 200 kV and used to acquire bright-field and dark-field images, selected area electron diffraction (SAED) patterns, and high-resolution images. The EDS analysis was done using a TEM Xplore detector from Oxford Instruments, UK. Analyzed samples consisted of sub-monolayers of ITO NPs deposited on  $\text{Si}_3\text{N}_4$  TEM grids (Norcada, AB, Canada).

X-ray diffraction (XRD) measurements were carried out using a Bruker (MA, USA) D8-Discover X-ray diffractometer with a Cu target ( $K_\alpha$  radiation, wavelength  $\lambda = 0.154$  nm) and a Göbel mirror to obtain a parallel beam configuration. All measurements were performed using grazing incidence X-ray

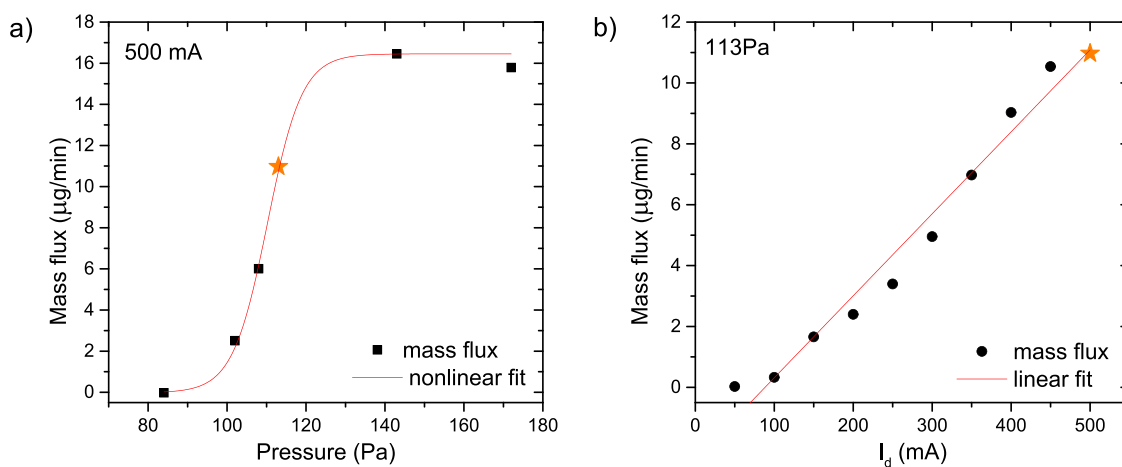


**Figure 2.** Mass flux ( $\mu\text{g}/\text{min}$ ) as a function of pressure (a) and discharge current (b). The effect of pressure in the aggregation chamber was tested under a constant discharge current of 500 mA, while the  $I_d$  effect was evaluated under a constant pressure of 113 Pa. The orange star indicates the experimental conditions chosen for the deposition of ITO NPs on substrates for subsequent characterizations.

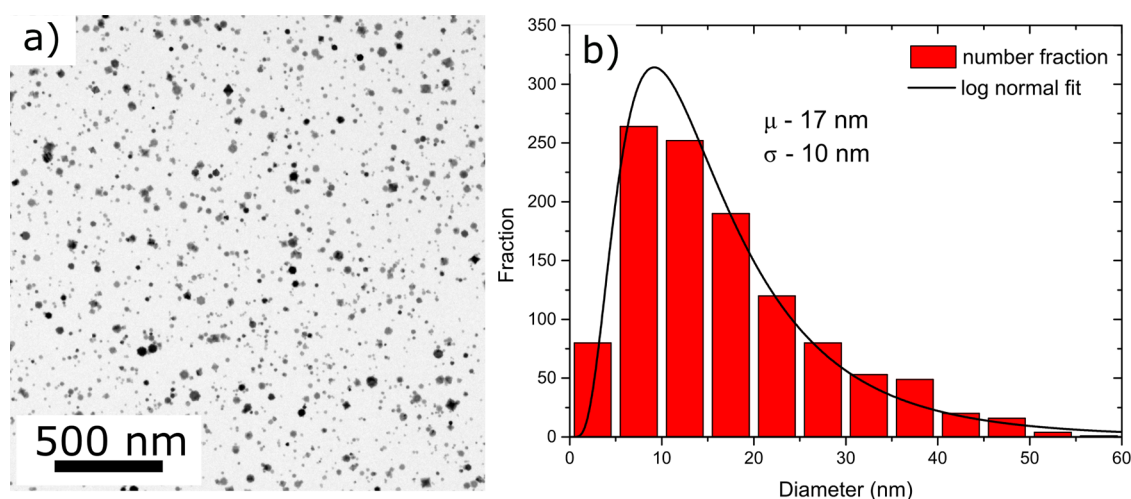


**Figure 3.** (a) TEM image of ITO NPs deposited at a pressure in the aggregation chamber of 113 Pa, an  $I_d$  of 500 mA, and a deposition time of 30 s; (b) size distribution of the NPs and log-normal fit.

diffraction (GIXRD). The diffraction patterns were evaluated using ICSD 50847 (similar to JCPDS card no. 06-0416).

## RESULTS AND DISCUSSION

**Deposition Rate.** In the first part of this work, we evaluated the deposition rate as one of the main parameters related to the flux of NPs toward the substrate as well as a fingerprint to adjust the growth kinetics and the process stability. As pointed out in previous works<sup>25,35,37–41</sup> on the GAS deposition method, the pressure in the aggregation chamber and discharge current are the main parameters affecting the deposition process of NPs. By regulating the Ar flow from 7 to 25 sccm while keeping the discharge current constant at 500 mA, a broad range of pressure values from 66 to 172 Pa was tested. The NPs were found to be created within the 84–172 Pa range with a nonlinear efficiency. Starting at 84 Pa, an increase in the working pressure leads to an abrupt increase in the deposition rate until about 120 Pa, where it starts to stabilize as indicated by the fitting of the experimental data in Figure 2a. This dependence denotes that higher deposition pressures promote the nucleation of ITO clusters, which may be explained by a more efficient thermal exchange of the vaporized target atoms with Ar atoms. At the same time, the occurrence of stabilization and even a slight decline suggest the onset of a shortage of fresh material supplied by the sputtering process, the yield of which is known to decrease at high deposition pressures.<sup>42</sup>

The impact of the discharge current,  $I_d$ , was tested under a fixed deposition pressure of 113 Pa, which was chosen as the most optimal value yielding a high deposition rate. In contrast to the deposition pressure, the effect of the discharge current was relatively straightforward. Starting from 100 mA, where the first ITO NPs were detected, the increase of the  $I_d$  stimulated an increase in the deposition rate up to a maximum value of 500 mA (Figure 2b). In the present sputtering configuration, where the working gas mixture is constant and the discharge voltage changes only slightly (210–234 V), the  $I_d$  directly affects the discharge power, which, in turn, predetermines the sputtering rate of ITO from the target. Thus, higher discharge currents supply more atoms and molecules that subsequently nucleate and form more ITO NPs.

Based on the mass flux analysis results, a deposition pressure of 113 Pa and an  $I_d$  of 500 mA (indicated with a star in Figure 2a) were chosen as the most representative and suitable conditions for the deposition and further characterization of the ITO NPs. These conditions also demonstrate a good run-to-run reproducibility that was evaluated by the optical response of the coatings, as described below.

### Morphology and Crystalline Structure of the NPs.

The size, shape, and crystalline structure of the ITO NPs were analyzed by TEM. A brief look at the TEM image shown in Figure 3a reveals the high uniformity of the NP coverage over the examined substrate surface. A statistical analysis, performed by using *ImageJ*, indicates the presence of ITO NPs with sizes varying from a few nanometers up to 60 nm. As can be seen in Figure 3b, the ITO NPs obey a log-normal distribution with a mean size ( $\mu$ ) of 17 nm and a standard deviation ( $\sigma$ ) of 10 nm. Another prominent parameter extracted from the statistical analysis of the TEM images was the flux ( $\Phi$ ) of the NPs to the substrate. Using the simple equation  $\Phi = N_{\text{total}}/(S \cdot t)$ , where  $N_{\text{total}}$  is the total number of NPs per area  $S$  ( $\mu\text{m}^2$ ) deposited for a period of time  $t$  (min), the resulting flux of ITO NPs is of 552 NPs/ $(\mu\text{m}^2 \cdot \text{min})$ , which is comparable to the flux of Cu NPs previously deposited by GAS.<sup>43</sup> Considering the linear relationship of the relative deposition rate with  $I_d$  (see Figure 2), the obtained  $\Phi$  value can be used to estimate the NP fluxes for other discharge current values (but only for a constant pressure of 113 Pa) in case it is needed for a specific application.

A high magnification TEM image, shown in Figure 4a, discerned various types of ITO NPs in terms of shape, which can be mainly divided into two groups: spherical and octahedron-like. A zoom-in into the single NPs of each type also revealed their different crystalline structures (Figure 4b–d). The octahedron-like NP possesses a single crystalline structure (Figure 4c), while some spherical NPs have either complex structures with a crystal core and amorphous shell (Figure 4c), or they are entirely amorphous, as seen in Figure 4d. Analysis of the SAED patterns reveals that all crystalline particles have a structure corresponding to cubic indium oxide. This conclusion is supported by the XRD results discussed below. The presence of amorphous ITO NPs suggests that it may be possible to crystallize them further using a post-annealing process.

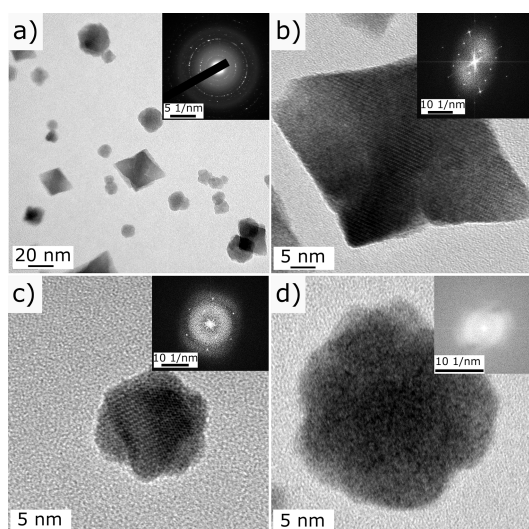


**Figure 4.** HRTEM images of ITO NPs revealing their different shapes and crystalline structures: (a) broad view of several NPs on the surface; (b) octahedron-like ITO NP; (c) spherical ITO NP with a complex partially crystalline structure; (d) spherical but completely amorphous ITO NP. The corresponding SAED pattern is shown in the inset of each image.

The XRD analysis of ITO NPs (Figure 5) demonstrated five very narrow diffraction peaks in the spectrum, confirming the

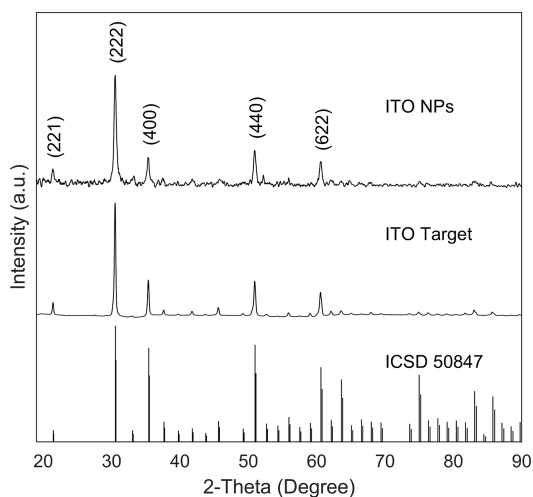


**Figure 5.** XRD spectrum of ITO NPs deposited at an  $I_d$  of 500 mA, a pressure of 113 Pa, and a deposition time of 30 min, XRD spectrum of the sputtered ITO target, and diffraction pattern of cubic  $\text{In}_2\text{O}_3$ , according to ICSD 50847.

highly crystalline nature of the ITO NPs as also indicated by TEM (see Figure 4). The XRD pattern of the NPs is equivalent to that of the ITO target, and it is in excellent agreement with the pattern of cubic  $\text{In}_2\text{O}_3$  from the database (ICSD 50847, similar to JCPDS card no. 06-0416). The most intense peaks were identified as the crystal planes (211), (222), (400), (440), and (622) of the cubic  $\text{In}_2\text{O}_3$  structure. The lack of signal from Sn and  $\text{SnO}_x$  species in the XRD spectrum suggests that Sn atoms replaced In atoms in the structure. A similar set of characteristic planes has been observed in previous works on ITO NPs prepared by the wet-chemistry methods.<sup>14,17</sup> Moreover, the present XRD pattern of our ITO

NPs is identical to the spectrum of a commercial ITO powder,<sup>44</sup> which, once again, points toward the resemblance of their crystalline structures.

Using Scherrer's equation  $t = (0.89\lambda)/(B\cos\theta)$ , where  $\lambda$  is the wavelength of the X-ray beam in the diffractometer,  $B$  is the full width at half-maximum of the strongest peak at the (222) plane, and  $\theta$  is the diffraction angle at the (111) plane, we obtain a crystallite size of 22.6 nm, which is in good agreement with the average size of the ITO NPs. In their recent work, Kim *et al.*<sup>17</sup> studied the effect of thermal annealing on ITO NPs and revealed that a larger grain size leads to a lower sheet resistance and higher conductivity of the NPs due to lower scattering at grain boundaries. Furthermore, they also demonstrated that the intensity ratio between the (222) and (400) peaks provides insight into the quality of the crystalline structure of the NPs, and confirmed that a higher ratio results in a lower sheet resistance of the coating. In our case, the XRD intensity line ratio is 3.84, close to the best-performing coatings in the range of 3.68–4.17 obtained in ref 17. for their samples annealed at 300–600 °C (the corresponding crystallite size varied within 10.35–11.85 nm). Thus, GAS enables the fabrication of highly crystalline ITO NPs without the need for post-deposition annealing. Moreover, the degree of crystallization and the shape of the NPs can most probably be controlled by the process parameters, for example, the discharge power. More investigation on this subject is needed.

**Chemical Composition.** The chemical composition of the ITO NPs was assessed by energy-dispersive X-ray spectroscopy (EDS). Benefiting from the TEM's analysis capabilities, we selected an area where only a single crystal octahedron NP or amorphous NP was present. For both types of NPs, the EDS analysis detected the core elements of ITO compounds such as In, Sn, and O with the corresponding atomic percentages summarized in Table 1. While absolute compositions in at.%

**Table 1.** EDS Elemental Composition of the Crystalline and Amorphous ITO NPs Shown in Figure 4b,d

	In, at.%	O, at.%	Sn, at.%	Sn/In	O/(Sn + In)
crystalline NP	16.0	82.4	1.6	10.0	4.6
amorphous NP	18.5	79.6	1.9	10.2	3.9

are far from the nominal chemical composition of the ITO target (Sn, 3.67%; In, 35.61%; O, 60.72%), an excellent agreement of the Sn/In ratio (10.0–10.2%) of ITO NPs with the original target material's ratio of 10.3% was revealed. The disagreement in the elemental composition can be particularly explained in terms of the O/(Sn + In) ratio. A quick look at the results indicates significantly large values of 4.6 and 3.9 compared to the nominal value of ~1.5. In the present case, the oxygen amount seems to be overestimated due to the contribution of signals from the adsorbed impurities on the substrate surface. Furthermore, due to the different sizes of the considered NPs, the NPs/substrate surface area ratios were slightly different during the EDS analysis, which may thus cause differences in the chemical composition between the NPs of different crystalline structures.

**Optical Properties.** The previously observed morphological and chemical characteristics of the produced ITO NPs suggest that they should indeed possess unique optical properties. For a complete optical characterization, we have chosen a sample deposited under identical deposition

conditions (113 Pa and 500 mA) but with a longer deposition time of 30 min. The analysis of the optical spectra shown in Figure 6a,c reveals a well-defined and strong absorption peak in

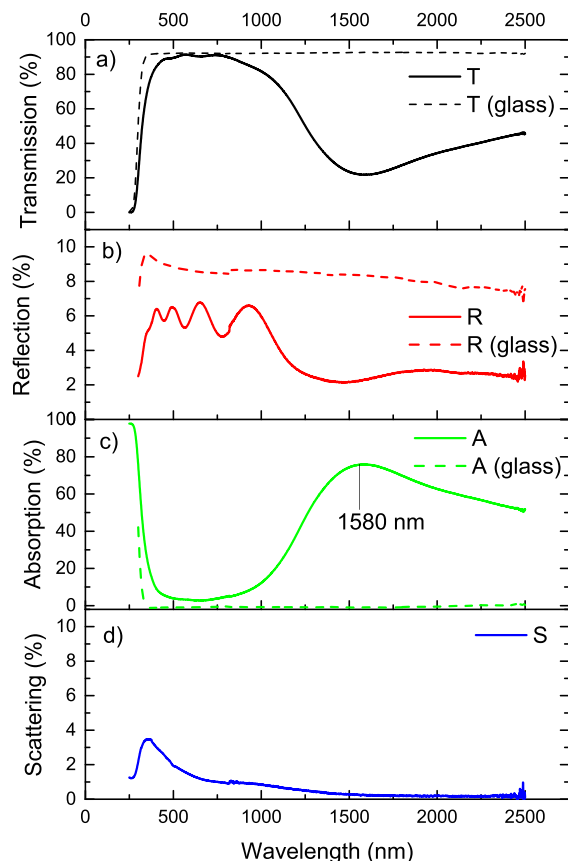


**Figure 6.** (a) Transmission, (b) reflection, (c) absorption, and (d) scattering spectra of ITO NPs deposited on a glass slide.

the near-infrared region positioned at 1580 nm. Remarkably, the previous wet-chemistry works on tuning the Sn doping in ITO NPs observed the same peak position for the NPs doped with 10% Sn.<sup>2,13,14</sup> Both works also demonstrated that 10% Sn is the most optimal percentage ensuring the highest density of free electrons, resulting in a shorter wavelength position and a higher absorption level of the plasmon peak. In our case, a maximum absorption of approximately 80% was achieved without affecting the visible spectrum (380–780 nm), as indicated by a high luminous transmittance ( $T_{lum}$ ) value of 91% (D65 illuminant and CIE 1931 2° observer). At the same time, the luminous reflectance decreased to 5.8% compared to 8.7% for the bare glass slide (Figure 6b).

Another crucial parameter that has often been overlooked by previous studies on ITO NPs is light scattering. Evaluation of scattering of the ITO NPs performed by an integrating sphere revealed a low haze level of around 1.7% at 550 nm (Figure 6d).

## CONCLUSIONS

The early results described in this paper demonstrate the outstanding potential for fabricating ITO NPs by the GAS method. It was found that a combination of high deposition pressure (>110 Pa) with high  $I_d$  (500 mA) creates the most optimal conditions for the fabrication of the ITO NPs. The optimized experimental conditions resulted in the formation of

ITO NPs with an average size of  $17 \pm 10$  nm, most of them possessing a highly crystalline structure identical to the target material. The chemical composition analysis revealed a similar Sn/In ratio but an increased concentration of oxygen in the NPs in comparison to the target material. The optical analysis showed the presence of a characteristic plasmon peak at 1580 nm and a maximum absorption of around 80%. Intense absorption in the near-infrared region did not affect the transmission in the visible part of the spectrum (380–780 nm), as demonstrated by the resulting high  $T_{lum}$  of 91%. Considering the complexity of the parameters affecting the properties of ITO material during its deposition, it is remarkable to achieve this optical performance by employing the most straightforward approach of sputtering an ITO target in Ar gas without external manipulations of the NPs.

Since this is the first work on the fabrication of the ITO NPs using the GAS method, we wish to highlight the priorities for further investigations. First, it is necessary to explore other opportunities to improve the optical properties of ITO NPs, such as adding a small amount of oxygen into the working gas mixture. The second aspect relates to improving the efficiency of the ITO NPs' optical response through initiating crystallization of the amorphous species that were observed in the deposit. It has been shown that exposing ITO NPs to high annealing temperatures (300–600 °C) in various gas atmospheres can significantly improve their absorption efficiency.<sup>17</sup> Finally, the compatibility of the GAS method with other vacuum-based deposition processes makes it possible to envision various nanocomposite coatings based on ITO NPs. For example, incorporating the ITO NPs into a material with electrochromic properties can allow one to independently tune the transmission in the visible and near-infrared regions.<sup>19</sup>

## AUTHOR INFORMATION

### Corresponding Author

Ludvik Martinu – Department of Engineering Physics,  
Polytechnique Montreal, Montreal, QC H3T 1J4, Canada;  
Email: ludvik.martinu@polymtl.ca

### Authors

Artem Shelemin – Department of Engineering Physics,  
Polytechnique Montreal, Montreal, QC H3T 1J4, Canada  
Zdenek Krtous – Department of Engineering Physics,  
Polytechnique Montreal, Montreal, QC H3T 1J4, Canada;  
Department of Macromolecular Physics, Faculty of  
Mathematics and Physics, Charles University, Prague 12000,  
Czech Republic  
Bill Baloukas – Department of Engineering Physics,  
Polytechnique Montreal, Montreal, QC H3T 1J4, Canada;  
[orcid.org/0000-0001-7263-0114](https://orcid.org/0000-0001-7263-0114)  
Oleg Zabeida – Department of Engineering Physics,  
Polytechnique Montreal, Montreal, QC H3T 1J4, Canada;  
[orcid.org/0000-0001-8103-9852](https://orcid.org/0000-0001-8103-9852)  
Jolanta Klemberg-Sapieha – Department of Engineering  
Physics, Polytechnique Montreal, Montreal, QC H3T 1J4,  
Canada

Complete contact information is available at:  
<https://pubs.acs.org/10.1021/acsomega.2c08070>

### Notes

The authors declare no competing financial interest.

## ACKNOWLEDGMENTS

The authors wish to thank Francis Turcot and Francis Boutet for their technical assistance and Dr. Luis Varela for his help with the XRD measurements. This work has been supported by the Natural Sciences and Engineering Research Council of Canada (NSERC) through the NSERC Multisectorial Industrial Research Chair in Coatings and Surface Engineering grant (IRCPJ 433808-11).

## REFERENCES

- (1) Kim, H.; Gilmore, C. M.; Piqué, A.; Horwitz, J. S.; Mattoussi, H.; Murata, H.; Kafafi, Z. H.; Chrisey, D. B. Electrical, Optical, and Structural Properties of Indium-Tin-Oxide Thin Films for Organic Light-Emitting Devices. *J. Appl. Phys.* **1999**, *86*, 6451–6461.
- (2) Park, D.; Park, W.; Song, J.; Kim, S. S. High-Performance ITO Thin Films for on-Cell Touch Sensor of Foldable OLED Displays. *J. Inf. Disp.* **2022**, *23*, 77–85.
- (3) Granqvist, C. G.; Hultåker, A. Transparent and Conducting ITO Films: New Developments and Applications. *Thin Solid Films* **2002**, *411*, 1–5.
- (4) Toušková, J.; Kovanda, J.; Dobiášová, L.; Pařezek, V.; Kielar, P. Sputtered Indium-Tin Oxide Substrates for CdSCdTe Solar Cells. *Sol. Energy Mater. Sol. Cells* **1995**, *37*, 357–365.
- (5) Du, J.; Chen, X.-L.; Liu, C.-C.; Ni, J.; Hou, G.-F.; Zhao, Y.; Zhang, X.-D. Highly Transparent and Conductive Indium Tin Oxide Thin Films for Solar Cells Grown by Reactive Thermal Evaporation at Low Temperature. *Appl. Phys. Mater. Sci. Process.* **2014**, *117*, 815–822.
- (6) Ren, Y.; Zhou, X.; Wang, Q.; Zhao, G. Novel Preparation of ITO Nanocrystalline Films with Plasmon Electrochromic Properties by the Sol-Gel Method Using Benzoylacetone as a Chemical Modifier. *Ceram. Int.* **2018**, *44*, 3394–3399.
- (7) Dong, L.; Zhu, G. S.; Xu, H. R.; Jiang, X. P.; Zhang, X. Y.; Zhao, Y. Y.; Yan, D. L.; Yuan, L.; Yu, A. B. Preparation of Indium Tin Oxide (ITO) Thin Film with (400) Preferred Orientation by Sol-Gel Spin Coating Method. *J. Mater. Sci.: Mater. Electron.* **2019**, *30*, 8047–8054.
- (8) Xia, N.; Gerhardt, R. A. Fabrication and Characterization of Highly Transparent and Conductive Indium Tin Oxide Films Made with Different Solution-Based Methods. *Mater. Res. Express* **2016**, *3*, 116408.
- (9) Fang, X.; Mak, C. L.; Zhang, S.; Wang, Z.; Yuan, W.; Ye, H. Pulsed Laser Deposited Indium Tin Oxides as Alternatives to Noble Metals in the Near-Infrared Region. *J. Phys. Condens. Matter* **2016**, *28*, 224009.
- (10) Prepelita, P.; Stavarache, I.; Craciun, D.; Garoi, F.; Negri, C.; Sbarcea, B. G.; Craciun, V. Rapid Thermal Annealing for High-Quality ITO Thin Films Deposited by Radio-Frequency Magnetron Sputtering. *Beilstein J. Nanotechnol.* **2019**, *10*, 1511–1522.
- (11) Kurdesau, F.; Khripunov, G.; da Cunha, A. F.; Kaelin, M.; Tiwari, A. N. Comparative Study of ITO Layers Deposited by DC and RF Magnetron Sputtering at Room Temperature. *J. Non-Cryst. Solids* **2006**, *352*, 1466–1470.
- (12) Wang, Y.; Overvig, A. C.; Shrestha, S.; Zhang, R.; Wang, R.; Yu, N.; Dal Negro, L. Tunability of Indium Tin Oxide Materials for Mid-Infrared Plasmonics Applications. *Opt. Mater. Express* **2017**, *7*, 2727.
- (13) Ma, K.; Zhou, N.; Yuan, M.; Li, D.; Yang, D. Tunable Surface Plasmon Resonance Frequencies of Monodisperse Indium Tin Oxide Nanoparticles by Controlling Composition, Size, and Morphology. *Nanoscale Res. Lett.* **2014**, *9*, 1–7.
- (14) Katagiri, K.; Takabatake, R.; Inumaru, K. Robust Infrared-Shielding Coating Films Prepared Using Perhydropolysilazane and Hydrophobized Indium Tin Oxide Nanoparticles with Tuned Surface Plasmon Resonance. *ACS Appl. Mater. Interfaces* **2013**, *5*, 10240–10245.
- (15) Garcia, G.; Buonsanti, R.; Runnerstrom, E. L.; Mendelsberg, R. J.; Llordes, A.; Anders, A.; Richardson, T. J.; Milliron, D. J. Dynamically Modulating the Surface Plasmon Resonance of Doped Semiconductor Nanocrystals. *Nano Lett.* **2011**, *11*, 4415–4420.
- (16) Kanehara, M.; Koike, H.; Yoshinaga, T.; Teranishi, T. Indium Tin Oxide Nanoparticles with Compositionally Tunable Surface Plasmon Resonance Frequencies in the Near-IR Region. *J. Am. Chem. Soc.* **2009**, *131*, 17736–17737.
- (17) Kim, C.; Park, J.-W.; Kim, J.; Hong, S.-J.; Lee, M. J. A Highly Efficient Indium Tin Oxide Nanoparticles (ITO-NPs) Transparent Heater Based on Solution-Process Optimized with Oxygen Vacancy Control. *J. Alloys Compd.* **2017**, *726*, 712–719.
- (18) Matsui, H.; Tabata, H. Assembled Films of Sn-Doped In<sub>2</sub>O<sub>3</sub> Plasmonic Nanoparticles on High-Permittivity Substrates for Thermal Shielding. *ACS Appl. Nano Mater.* **2019**, *2*, 2806–2816.
- (19) Korgel, B. A. Composite for Smarter Windows. *Nature* **2013**, *500*, 278–279.
- (20) Granqvist, C. G. Electrochromics for Smart Windows: Oxide-Based Thin Films and Devices. *Thin Solid Films* **2014**, *564*, 1–38.
- (21) Yoon, S.; Kim, H.; Cha, S. J.; Shin, E. S.; Noh, Y. Y.; Hong, S. J.; Park, B.; Hwang, I. Role of ITO Nanoparticles Embedded into Electrospun ITO Nanofibers. *J. Phys. D: Appl. Phys.* **2017**, *50*, 475305.
- (22) Otanicar, T. P.; DeJarnette, D.; Hewakuruppu, Y.; Taylor, R. A. Filtering Light with Nanoparticles: A Review of Optically Selective Particles and Applications. *Adv. Opt. Photon.* **2016**, *8*, 541.
- (23) Drábik, M.; Choukourov, A.; Artemenko, A.; Kousal, J.; Polonskyi, O.; Solař, P.; Kylián, O.; Matoušek, J.; Pešička, J.; Matolénová, I.; Slavěnská, D.; Biederman, H. Morphology of Titanium Nanocluster Films Prepared by Gas Aggregation Cluster Source. *Plasma Processes Polym.* **2011**, *8*, 640–650.
- (24) Kousal, J.; Shelemin, A.; Schwartzkopf, M.; Polonskyi, O.; Hanaš, J.; Solař, P.; Vaidulych, M.; Nikitin, D.; Pleskunov, P.; Krtouš, Z.; Strunskus, T.; Faupel, F.; Roth, S. V.; Biederman, H.; Choukourov, A. Magnetron-Sputtered Copper Nanoparticles: Lost in Gas Aggregation and Found by in Situ X-Ray Scattering. *Nanoscale* **2018**, *10*, 18275–18281.
- (25) Kylián, O.; Valeš, V.; Polonskyi, O.; Pešička, J.; Čechvala, J.; Solař, P.; Choukourov, A.; Slavěnská, D.; Biederman, H. Deposition of Pt Nanoclusters by Means of Gas Aggregation Cluster Source. *Mater. Lett.* **2012**, *79*, 229–231.
- (26) Shelemin, A.; Kylián, O.; Hanaš, J.; Choukourov, A.; Melnichuk, I.; Serov, A.; Slavěnská, D.; Biederman, H. Preparation of Metal Oxide Nanoparticles by Gas Aggregation Cluster Source. *Vacuum* **2015**, *120*, 162–169.
- (27) Shelemin, A.; Nikitin, D.; Choukourov, A.; Kylián, O.; Kousal, J.; Khalakhan, I.; Melnichuk, I.; Slavěnská, D.; Biederman, H. Preparation of Biomimetic Nano-Structured Films with Multi-Scale Roughness. *J. Phys. D: Appl. Phys.* **2016**, *49*, 254001.
- (28) Marek, A.; Valter, J.; Kadlec, S.; Vyskočil, J. Gas aggregation nanocluster source — Reactive sputter deposition of copper and titanium nanoclusters. *Surf. Coat. Technol.* **2011**, *205*, S573–S576.
- (29) Choukourov, A.; Pleskunov, P.; Nikitin, D.; Titov, V.; Shelemin, A.; Vaidulych, M.; Kuzminova, A.; Solař, P.; Hanaš, J.; Kousal, J.; Kylián, O.; Slavěnská, D.; Biederman, H. Advances and Challenges in the Field of Plasma Polymer Nanoparticles. *Beilstein J. Nanotechnol.* **2017**, *8*, 2002–2014.
- (30) Pleskunov, P.; Nikitin, D.; Tafichuk, R.; Shelemin, A.; Hanaš, J.; Kousal, J.; Krtouš, Z.; Khalakhan, I.; Kůš, P.; Nasu, T.; Nagahama, T.; Funaki, C.; Sato, H.; Gawek, M.; Schoenhals, A.; Choukourov, A. Plasma Polymerization of Acrylic Acid for the Tunable Synthesis of Glassy and Carboxylated Nanoparticles. *J. Phys. Chem. B* **2020**, *124*, 668–678.
- (31) Hanaš, J.; Vaidulych, M.; Kylián, O.; Choukourov, A.; Kousal, J.; Khalakhan, I.; Cieslar, M.; Solař, P.; Biederman, H. Fabrication of Ni@Ti Core-Shell Nanoparticles by Modified Gas Aggregation Source. *J. Phys. D: Appl. Phys.* **2017**, *50*, 475307.
- (32) Kretková, T.; Hanaš, J.; Kylián, O.; Solař, P.; Dopita, M.; Cieslar, M.; Khalakhan, I.; Choukourov, A.; Biederman, H. In-Flight Modification of Ni Nanoparticles by Tubular Magnetron Sputtering. *J. Phys. D: Appl. Phys.* **2019**, *52*, 205302.
- (33) Kylián, O.; Shelemin, A.; Solař, P.; Pleskunov, P.; Nikitin, D.; Kuzminova, A.; Štefaněková, R.; Kůš, P.; Cieslar, M.; Hanaš, J.; Choukourov, A.; Biederman, H. Magnetron Sputtering of Polymeric

Targets: From Thin Films to Heterogeneous Metal/Plasma Polymer Nanoparticles. *Materials* **2019**, *12*, 2366.

(34) Kylián, O.; Štefaněková, R.; Kuzminova, A.; Hanuš, J.; Solař, P.; Kůš, P.; Cieslar, M.; Biederman, H. In-Flight Plasma Modification of Nanoparticles Produced by Means of Gas Aggregation Sources as an Effective Route for the Synthesis of Core-Satellite Ag/Plasma Polymer Nanoparticles. *Plasma Phys. Control. Fusion* **2020**, *62*, No. 014005.

(35) Haberland, H. History, Some Basics, and an Outlook. In *Gas-Phase Synthesis of Nanoparticles*, Huttel, Y., Ed.; John Wiley & Sons, Ltd. 2017; pp. 23–38. DOI: 10.1002/9783527698417.ch1.

(36) Mecea, V. M. Fundamentals of Mass Measurements. *J. Therm. Anal. Calorim.* **2006**, *86*, 9–16.

(37) Kuzminova, A.; Beranová, J.; Polonskyi, O.; Shelemin, A.; Kylián, O.; Choukourov, A.; Slavěnská, D.; Biederman, H. Antibacterial Nanocomposite Coatings Produced by Means of Gas Aggregation Source of Silver Nanoparticles. *Surf. Coat. Technol.* **2016**, *294*, 225–230.

(38) Solař, P.; Kylián, O.; Marek, A.; Vandrovcová, M.; Bačáková, L.; Hanuš, J.; Vyskočil, J.; Slavěnská, D.; Biederman, H. Particles Induced Surface Nanoroughness of Titanium Surface and Its Influence on Adhesion of Osteoblast-like MG-63 Cells. *Appl. Surf. Sci.* **2015**, *324*, 99–105.

(39) Shelemin, A.; Pleskunov, P.; Kousal, J.; Drewes, J.; Hanuš, J.; Ali-Ogly, S.; Nikitin, D.; Solař, P.; Kratochvěl, J.; Vaidulych, M.; Schwartzkopf, M.; Kylián, O.; Polonskyi, O.; Strunskus, T.; Faupel, F.; Roth, S. V.; Biederman, H.; Choukourov, A. Nucleation and Growth of Magnetron-Sputtered Ag Nanoparticles as Witnessed by Time-Resolved Small Angle X-Ray Scattering. *Part. Part. Syst. Charact.* **2020**, *37*, 1–11.

(40) Popok, V. N.; Kylián, O. Gas-Phase Synthesis of Functional Nanomaterials. *Appl. Nano* **2020**, *1*, 25–58.

(41) Nikitin, D.; Hanuš, J.; Ali-Ogly, S.; Polonskyi, O.; Drewes, J.; Faupel, F.; Biederman, H.; Choukourov, A. The Evolution of Ag Nanoparticles inside a Gas Aggregation Cluster Source. *Plasma Processes Polym.* **2019**, *16*, 1900079.

(42) Gudmundsson, J. T. Physics and Technology of Magnetron Sputtering Discharges. *Plasma Sources Sci. Technol.* **2020**, *29*, 113001.

(43) Vaidulych, M.; Shelemin, A.; Hanuš, J.; Khalakhan, I.; Krakovsky, I.; Kočová, P.; Mašková, H.; Kratochvěl, J.; Pleskunov, P.; Štěrba, J.; Kylián, O.; Choukourov, A.; Biederman, H. Superwetable Antibacterial Textiles for Versatile Oil/Water Separation. *Plasma Processes Polym.* **2019**, *16*, 1900003.

(44) Cho, Y.-S.; Jeong, S.; Nam, S. Stable Dispersion of ITO Nanoparticles for Self-Organization by Electrospinning and Electro-spray. *J. Dispersion Sci. Technol.* **2020**, *41*, 1963–1975.